ELSEVIER

Available online at www.sciencedirect.com

SCIENCE DIRECT®

Microelectronic Engineering 82 (2005) 154–167

MICROELECTRONIC ENGINEERING

www.elsevier.com/locate/mee

Embedded benzocyclobutene in silicon: An integrated fabrication process for electrical and thermal isolation in MEMS

Alireza Modafe, Nima Ghalichechian, Michael Powers, Michael Khbeis, Reza Ghodssi *

MEMS Sensors and Actuators Laboratory (MSAL), Department of Electrical and Computer Engineering, The Institute for Systems Research, University of Maryland, 2410 A.V. Williams Building, College Park, MD 20742, United States

Received 14 June 2005; received in revised form 6 July 2005; accepted 6 July 2005
Available online 2 August 2005

Abstract

This paper reports a novel fabrication process to develop planarized isolated islands of benzocyclobutene (BCB) polymer embedded in a silicon substrate. Embedded BCB in silicon (EBiS) can be used as an alternative to silicon dioxide in fabrication of electrostatic micromotors, microgenerators, and other microelectromechanical devices. EBiS takes advantage of the low dielectric constant and thermal conductivity of BCB polymers to develop electrical and thermal isolation integrated in silicon. The process involves conventional microfabrication techniques such as photolithography, deep reactive ion etching, and chemical mechanical planarization (CMP). We have characterized CMP of BCB polymers in detail since CMP is a key step in EBiS process. Atomic force microscopy (AFM) and elipsometry of blanket BCB films before and after CMP show that higher polishing down force pressure and speed lead to higher removal rate at the expense of higher surface roughness, non-uniformity, and scratch density. This is expected since BCB is a softer material compared to inorganic films such as silicon dioxide. We have observed that as the cure temperature of BCB increases beyond 200 °C, the CMP removal rate decreases drastically. The results from optical microscopy, scanning electron microscopy, and optical profilometry show excellent planarized surfaces on the EBiS islands. An average step height reduction of more than 95% was achieved after two BCB deposition and three CMP steps.
© 2005 Elsevier B.V. All rights reserved.

Keywords: Benzocyclobutene; BCB; MEMS; Electrical isolation

* Corresponding author. Tel.: +1 301 405 8158; fax: +1 301 314 9281.
E-mail address: ghodssi@eng.umd.edu (R. Ghodssi).

0167-9317/$ - see front matter © 2005 Elsevier B.V. All rights reserved.
doi:10.1016/j.mee.2005.07.005

1. Introduction

Electrical and thermal isolation, as well as physical properties of dielectric materials, play an increasingly important role in the performance, efficiency, and reliability of microelectromechanical systems (MEMS). The range of dielectric materials and isolation techniques in MEMS has grown, especially in recent years. Traditionally, silicon dioxide has been and still is used for insulation in microelectronics and MEMS. Recent advances in the area of power MEMS [1,2] include a significant number of research activities on development of crack-free, low-stress, and thick silicon dioxide films [3–5]. In addition to electrical insulation, thick silicon dioxide has been used for high-frequency [6] and thermal [7,8] isolation. The drawbacks of silicon dioxide as an insulating film for MEMS applications include high dielectric constant, limited thickness due to high residual stress, and high-temperature process, which affects the performance, efficiency, and reliability [9].

Low-dielectric-constant (low-k) polymers based on benzocyclobutene (BCB) [10,11] have several advantages over silicon dioxide for variety of applications, including electrical and thermal isolation in MEMS. BCB polymers ere primarily used as an interlayer dielectric (ILD) for microelectronic applications [12], and more recently for low-temperature adhesive wafer bonding [13] and as a structural material [14] in MEMS. BCB polymers are commercially available in the form of partially cured BCB monomers in mesitylene solvent under a trademark name (Cyclotene) from Dow Chemical (Midland, MI).

Table 1 compares common physical properties of silicon dioxide and those of BCB polymers. The lower dielectric constant of BCB polymers ($k = 2.65$) in combination with employing a thicker film leads to lower parasitic capacitances, and as a result, to lower electrical energy loss in electrostatically driven MEMS. The higher volume resistivity of BCB polymers ($\rho = 10^{19}\ \Omega\,\mathrm{cm}$) reduces the leakage current through the insulating layers.

Table 1
Physical properties of BCB polymers and silicon dioxide (at 25 °C unless otherwise noted) [BCB properties from manufacturer's data sheets]

Physical properties	SiO_2	BCB polymer
Dielectric constant	3.9	2.65 (hard-cured)
Dissipation factor	0.0002	0.0008–0.002 (at 1 MHz to 10 GHz)
Dielectric strength (V/cm)	$6–9 \times 10^6$	3×10^6
Volume resistivity (Ω cm)	1×10^{14}	1×10^{19}
Tensile strength (MPa)	69–276	85 ± 9 (dry-etch) 87 ± 9 (photo)
Tensile modulus (GPa)	73	2.0 ± 0.2 (dry-etch) 2.9 ± 0.2 (photo)
Tensile elongation (%)	N/A	8 ± 2.5 (at break)
Poisson ratio	0.17	0.34
Residual stress on Si (MPa)	100–300 (comp.)	28 ± 2 (tensile)
Thermal conductivity (W/m K)	1.4	0.29
Specific heat (J/kg K)	1400	2180
CTE (ppm/°C)	0.5	52 (at 25–300 °C)
Transition temperature	1710 °C (melting)	350 °C (glass transition)
Thermal stability (% weight loss/h)	N/A	1.6 (at 350 °C)
Index of refraction	1.46	1.54 (hard-cured) (at 1300–1550 nm)
Density (g/cm^3)	2.19	1.05 (hard-cured)
Moisture uptake (%)	N/A	0.13 (dry-etch, at 81%RH) 0.14 (photo, at 84%RH)
Shrinkage (%)	N/A	<5 (hard-cured)
Planarization (%)	N/A	>90

The thermal conductivity of BCB polymers ($\kappa = 0.29$ W/m K) is five times smaller than that of silicon dioxide, making BCB polymer a much better thermal insulator. Furthermore, the residual stress of BCB polymer films is one order of magnitude smaller than that of silicon dioxide. This allows the use of very thick BCB polymer films with little concerns about wafer bow and film crack, which are major problems in application of thick silicon dioxide films. In addition, deposition process of BCB polymers includes simple spin-coating and low-temperature curing compared to more complicated and more expensive deposition techniques for silicon dioxide. Although the glass transition temperature of BCB polymers ($T_g = 350$ °C) is much lower than the melting point of silicon dioxide ($T_m = 1710$ °C), they can be used in a variety of low- to moderate-temperature applications in MEMS. BCB polymers are also prone to moisture uptake, which can affect their physical properties. In our previous work [9], we have experimentally shown that the dielectric constant of BCB polymers does not change appreciably with moisture uptake, while their current–voltage characteristics (e.g., leakage current and breakdown voltage) are degraded. For example, we have shown that the breakdown voltage of BCB polymer films is reduced from 300 to 100 V/μm after a humidity stress test. This could be a limiting factor in some applications that a thin BCB film is used for electrical isolation of high voltages. The technique introduced in this paper, however, uses a thick BCB film for isolation and can provide electrical isolation of thousands of volts even after moisture uptake.

Integration of BCB polymer films with conventional MEMS processes such as silicon bulk micromachining is not a trivial task, mainly because the polymer cannot withstand the harsh condition of some chemical environments, especially hot potassium hydroxide (KOH). The poor adhesion of the BCB polymers to metals and other inorganic films makes the integration even more challenging. Thin BCB polymer film (~1 μm) has been successfully integrated with micromachined silicon v-grooves [15], while integration of thick BCB polymer films is still facing the challenge of polymer undercutting during silicon etching.

We have developed a novel technique called embedded BCB in silicon (EBiS) to take advantage of the unique features of BCB polymer films for electrical and thermal isolation and to integrate these films with other microfabricated structures and devices [16]. The objective of EBiS process is to develop planarized isolated islands of thick BCB polymer films embedded in a silicon substrate. These islands act as the insulating beds for active areas, where subsequent devices and structures are fabricated. As an example, one application area of EBiS is bottom-drive electrostatic micromotors, where the electrodes and interconnects of the stator are insulated from the substrate using EBiS islands [17]. A schematic of the final silicon wafer after development of EBiS islands is shown in Fig. 1. The EBiS process is an alternative to the conventional method where a thick dielectric film such as silicon dioxide is deposited across the wafer, patterned if necessary, and subsequent layers and structures are fabricated on top of the film. There are several advantages for the EBiS process over the conventional method:

(i) The overall wafer bow is reduced because the residual stress is limited to small embedded islands compared to a blanket film across the wafer.
(ii) The polymer film and the associated problems such as etching, adhesion, etc. in areas outside the islands are minimized;

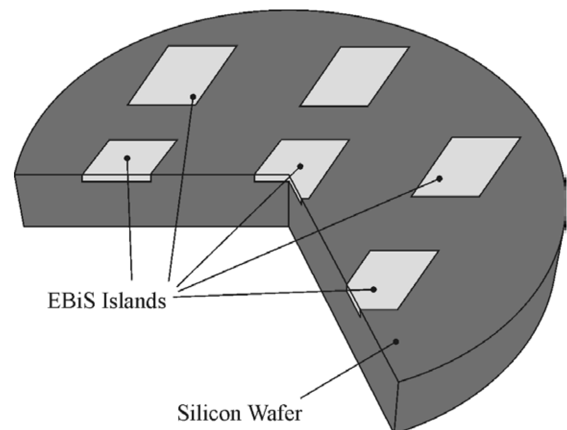

Fig. 1. A schematic of a silicon wafer with several planarized embedded BCB in silicon (EBiS) islands.

(iii) The subsequent fabrication processes are less prone to fabrication defects, leading to higher yields because the islands are highly planarized.
(iv) Since the polymer layer is embedded in the substrate, the adhesion of the polymer to the substrate is improved compared to blanket film.
(v) The overall adhesion of the metal films to the substrate is improved by limiting the polymer to a small area on the substrate.
(iv) In case of etching silicon v-grooves in hot KOH, the polymer can be completely masked with a metal layer to prevent undercut.

The EBiS process is adopted from thick buried oxide in silicon (TBOS) process [3]. TBOS is a fabrication process developed to create isolated islands of plasma-enhanced chemical vapor deposited (PECVD) silicon dioxide to reduce the overall wafer bow for subsequent wafer bonding. EBiS, however, enables the incorporation of spin-on, thick BCB polymer films in silicon substrate, leading to excellent electrical and thermal isolation, lower electrical energy loss, lower residual stress and wafer bow, and easier fabrication and process integration.

This paper introduces the EBiS process as an enabling tool for electrical and thermal isolation in fabrication of MEMS. Since chemical mechanical planarization (CMP) of BCB polymers is a key process step in EBiS, Sections 2 and 3 review the CMP process, its parameters, the specifics of this study, and presents the characterization results for CMP of blanket BCB polymer films. In Section 4, we will go over the EBiS fabrication process, present fabrication results, and discuss measurement data. Finally, Section 5 provides concluding remarks.

2. Planarization of BCB polymers

The surface of the wafer is globally planarized during the EBiS process, although BCB polymers are excellent planarizers with a degree of planarization (DOP) of about 95% when coated over isolated, shallow trenches [12]. The planarization of BCB polymers in EBiS process is achieved using CMP, which is the de facto standard for global planarization in integrated circuit chip fabrication today [18].

CMP is a planarization method that uses a combination of mechanical abrasion and chemical etching to physically remove material from places of high topography and flatten the wafer surface. In all experiments presented in this paper, a 6EC CMP tool from Strasbaugh (San Luis Obispo, CA) was used for polishing the wafers.

The output parameters that are commonly used to benchmark a CMP process are removal rate, removal uniformity, removal selectivity, and surface topography of the polished film. These parameters are the result of mechanical and chemical interaction at the interface of three major components of a CMP process: polishing pad, polishing slurry, and wafer. There are several variables that affect these interactions and control the output parameters, making the CMP process a complicated phenomenon to analyze and model. Table 2 summarizes some of the control parameters and the affected output parameters in a generic CMP process [19].

The control parameters of CMP are not limited to those listed in Table 2. For instance, the parameters of pad conditioning can greatly impact the polishing results. Some CMP tools (including 6EC) allow the user to apply a back pressure (positive or negative) on the wafer to compensate for

Table 2
CMP control and output parameters

Control parameter	Output parameter
Down force pressure	RR[a], RU[b], RS[c]
Wafer carrier rotation speed	RR, RU, RS
Platen rotation speed	RR, RU, RS
Slurry chemistry	RR, RS, ST[d]
Slurry abrasive (type, size, percent)	RR, RS, ST
Pad hardness	RR, RU, RS, ST
Pad porosity	RU
Wafer carrier film hardness	RU

[a] RR, removal rate.
[b] RU, removal uniformity.
[c] RS, removal selectivity.
[d] ST, surface topography.

the wafer bow or apply a pressure to the retaining ring to adjust the polish of the wafer edge. Platen temperature, slurry flow rate, and polishing time also affect the output parameters. The most important control parameters are down force pressure, platen rotation speed, and wafer carrier rotation speed. These parameters determine the removal rate of the film based on the empirical Preston equation [20]

$$\mathrm{RR} = K_{\mathrm{p}}PV, \tag{1}$$

where RR is the removal rate, V is the linear velocity of the platen relative to the wafer, P is the down force pressure pressing the wafer onto the pad, and K_{p} is the Preston coefficient. The Preston coefficient is a function of the mechanical and chemical properties of the polishing pad, slurry, and the film being polished. Considering only the mechanical properties of the film, it has been shown that the Preston coefficient is inversely proportional to the Young's modulus of the film [21]

$$K_{\mathrm{p}} = \frac{1}{2E}, \tag{2}$$

where E is the Young's modulus of the film being polished. It has also been shown that (1) mostly applies to hard-pad CMP systems while RR is proportional to $P^{1.5}$ instead of P for soft-pad CMP systems [22]. More complete and accurate CMP models can be found in the literature [23–29].

CMP of polymer materials such as BCB polymers is more challenging than inorganic materials such as silicon dioxide and metals. Some specific properties of BCB polymers result in observation of distinct phenomena during CMP process: (i) BCB polymers are known to have hydrophobic surfaces [30], resulting in low surface reactivity and low removal rate; (ii) the hardness of the polymers is lower than that of inorganic materials, leading to high levels of scratching and post-CMP defects; (iii) the low hardness of the polymers can also result in embedded abrasive particles in the polished film and (iv) the level of polymer cross-linking is a function of cure temperature and time. Therefore, the hardness and surface reactivity of BCB polymers, and as a result their removal rate, strongly depend on cure temperature and time.

3. Characterization of CMP for BCB polymers

Considering the challenges in planarization of BCB polymers, it is important to understand the behavior of blanket BCB polymer films in CMP process before characterizing the CMP process for more complicated structures such as EBiS islands. Furthermore, such characterization can help with the design and optimization of the EBiS process. For these reasons, we conducted a series of experiments to study and characterize the CMP process for BCB polymers. In this characterization, we were mainly interested in the difference between parameters of uncured and cured films, such as removal rate, non-uniformity, and surface topography.

The physical properties of dry-etch and photosensitive BCB polymers, as Table 1 shows, have minor differences. Therefore, the characterization samples were prepared with the dry-etch (non-photosensitive) BCB polymer (Cyclotene 3022-63) instead of the photosensitive BCB polymer (Cyclotene 4026-46), which is used in the EBiS process. All samples were 4″ silicon wafers and prepared in the following manner. Each wafer was dehydrated at 130 °C for 10 min on a hotplate. AP3000, an adhesion promoter developed for Cyclotene by Dow Chemical, was dispensed and spun onto the wafer at 3000 rpm for 30 s. Next, Cyclotene 3022-63 was dispensed and spun onto the wafer, first at 500 rpm for 8 s and then, at 5000 rpm for 30 s. The sample was then baked at 85 °C for 150 s on hotplate. This was only done to drive out the remaining solvent. Several wafers were prepared and cured at different temperatures to study the effect of cure temperature on CMP parameters.

All wafers in this study were polished in our 6EC CMP tool with a k-grooved IC-1000 pad stacked on a SUBA IV pad from Rohm and Haas Electronic Materials (Phoenix, AZ). The specifications of the slurries used in this research, MSW2000A from Rohm and Haas Electronic Materials and ILD1300 from Nitta Haas Incorporated (Osaka, Japan), are listed in Table 3. Table 4 shows the polishing and pad conditioning parameters of the two CMP recipes that we used for polishing wafers.

Table 3
Specifications of CMP slurries

Specifications	MSW2000A	ILD1300
Primary target material	Tungsten	SiO_2
Abrasive material	Alumina	Silica
Median diameter of particles (nm)	170	175
Percentage of abrasives	28	13
Solution	Proprietary	NH_4OH
pH (at 25 °C)	3.9	10.75
Specific gravity (at 25 °C)	1.25 g/cm^3	1.07 g/cm^3

Table 4
CMP recipes

Input parameters	Recipe I	Recipe II
Polishing		
Down force pressure (psi)	2	3
Platen rotation speed (rpm)	34	120
Carrier rotation speed (rpm)	27	114
Backside pressure	0	0
Slurry flow rate (ml/min)	250	250
Pad conditioning		
Sweep type	In situ	
Sweep cycle	3 sweeps/cycles	
Platen rotation speed (rpm)	30	
Carrier rotation speed (rpm)	25	
Stroke pause (s)	30	
Slurry flow rate (ml/min)	75	

Initial polishing experiments were conducted using MSW2000A slurry with both recipes I and II. Fig. 2 shows atomic force microscopy (AFM) scans of soft-cured (cured at 210 °C for 40 min) BCB polymer surface before and after CMP with MSW2000A slurry using recipes I and II. Recipe I uses lower down force pressure and rotation speed, yielding lower removal rate but better uniformity, less defects, and better surface quality. Recipe II uses higher pressure and rotation speed, yielding higher removal rate but less uniformity, more scratches, and higher surface roughness. However, both recipes resulted in substantial embedded abrasive particles in the film.

Table 5 summarizes the quantitative data before and after CMP with each recipe. As seen in Table 5, the removal rate of the cured film is very low but the non-uniformity and surface roughness increases dramatically after CMP. This is most likely because the removal of BCB with MSW2000A results from mechanical abrasion rather than chemical etching. This is expected because, as Table 4 shows the percentage of abrasive particles in MSW2000A is relatively high, and the solution is acidic. We have observed that BCB polymers exhibit more resistance to acids than bases. It has been experimentally shown that adding surface-active agents (surfactants) such as Triton-X 100 to some slurries can improve the removal rate [30]. An alternative approach in some applications is to perform CMP on uncured or partially cured BCB polymers because the lower level of cross-linking can provide a higher removal rate. Furthermore, since BCB exhibits poor chemical resistance to bases [15], slurries with high pH (basic solutions), such as ILD1300, can potentially produce higher removal rates. Another advantage of ILD1300 over MSW2000A is its lower percentage of abrasive particles, which reduces the post-CMP scratches and embedded particles. Most experiments and processes in this study were conducted using ILD1300 and Recipe I because they produced the overall best results.

In order to study the performance of ILD1300 slurry and the effect of cure temperature, three samples were prepared. One wafer was left uncured and two other wafers were cured at two different temperatures below and above 200 °C, which is the activation temperature of BCB polymerization [31,32]. The exact cure temperatures are listed in Table 6. Note that that the higher cure temperature is close to the standard hard-cure (250 °C) temperature recommended for BCB polymers.

Fig. 3 shows AFM scans of uncured and cured BCB before and after CMP with ILD1300 slurry and recipe I. It is clear from Fig. 3(a) and (b) that embedded particle density is less compared to MSW2000A slurry (see Fig. 2). The scratch density is much higher in Fig. 3(b) because the BCB is cured at much lower temperature (188 °C). As shown in Fig. 3(c) the embedded particle density is high in case of uncured BCB. Comparing Fig. 3(a)–(c) reveals that scratch and embedded particle density is a function of cure temperature. Table 6 summarizes the quantitative data before and after CMP. The removal rate of BCB is extremely low at temperatures above 200 °C and

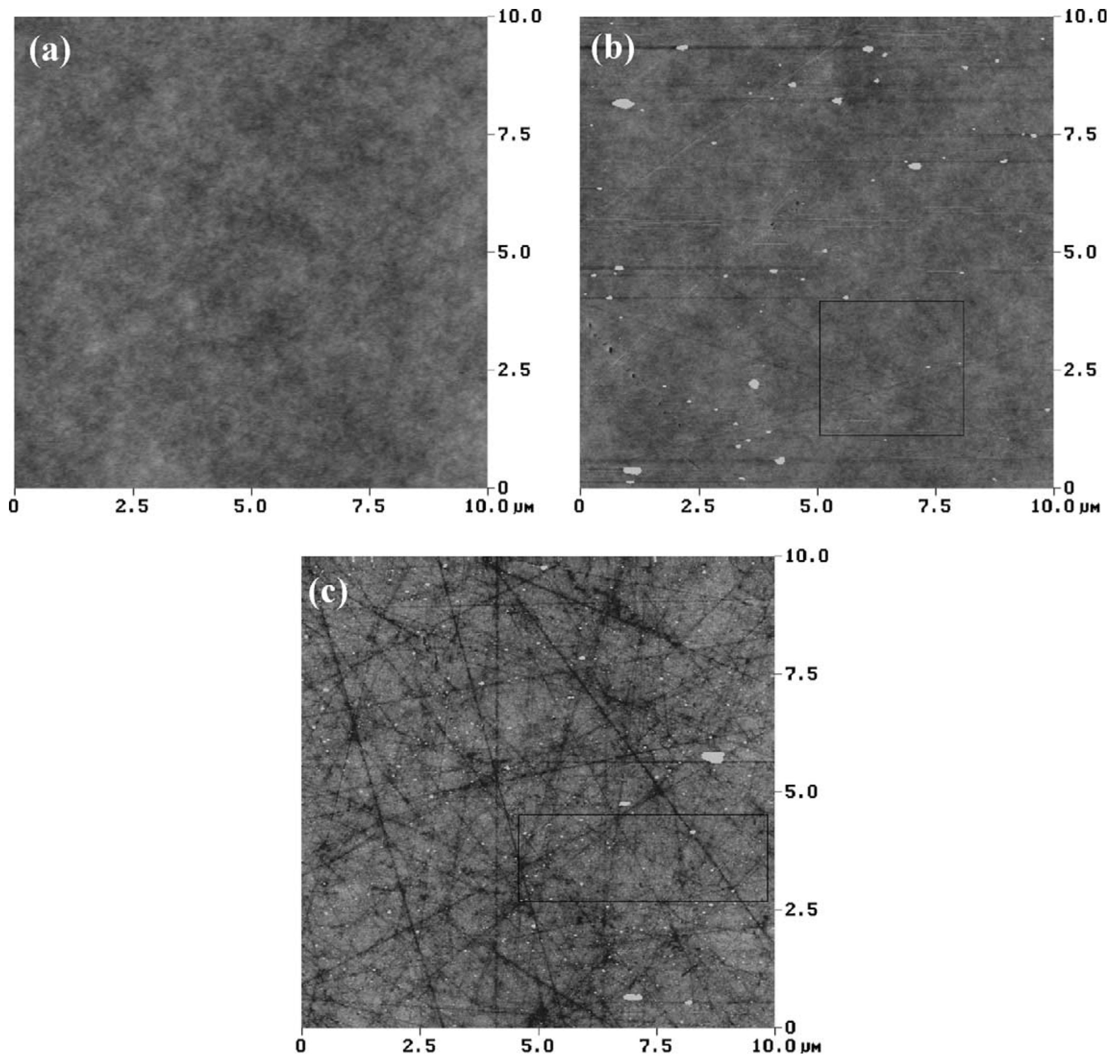

Fig. 2. AFM scans of BCB polymer surface cured at 210 °C showing the effect of CMP with MSW2000A slurry: (a) before CMP; (b) after CMP with recipe I; (c) after CMP with recipe II.

Table 5
Specifications of soft-cured BCB film before and after CMP with MSW2000A slurry and recipes I and II

Parameters	Pre-CMP	Recipe I	Recipe II
Polishing time (s)	N/A	120	120
Non-uniformity (%)	0.3	0.8	1.8
Removal rate (nm/min)	N/A	7	45
P–P roughness (Å)	41	1383	1511
Mean roughness (Å)	4	7	12
RMS roughness (Å)	5	29	33

increases as the cure temperature decreases below 200 °C. The removal rate is quite high for uncured BCB. The surface roughness of the film decreases after CMP for cure temperatures above 200 °C while it increases as the cure temperature goes below 200 °C. This shows that the CMP characteristics of BCB film are determined by the cure temperature, so that by controlling the level of polymerization through cure temperature, the output parameters of CMP process can be adjusted.

Table 6
CMP of BCB polymer cured at different temperatures using ILD1300 slurry and recipe I

Parameters	Wafer #1 (uncured)		Wafer #2 (cured @ 188 °C, 50 min)		Wafer #3 (cured @ 255 °C, 70 min)	
	Pre	Post	Pre	Post	Pre	Post
Mean thickness (μm)	10.43	6.46	9.36	9.33	9.31	9.30
Non-uniformity (%)	1.1	3.3	0.9	1.4	0.6	0.5
Polishing time (s)	N/A	65	N/A	305	N/A	305
Removal rate (nm/min)	N/A	3663	N/A	6.8	N/A	3.2
P–P roughness (Å)	32	1884	41	661	58	44
Mean roughness (Å)	3	31	4	6	4	1
RMS roughness (Å)	3	67	5	13	5	2

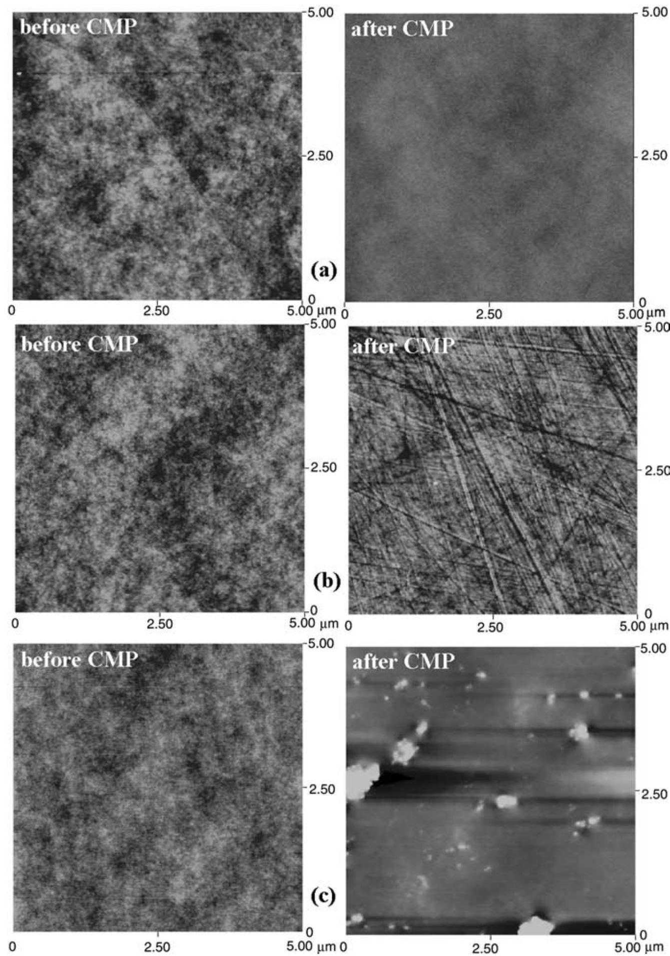

Fig. 3. AFM scans of BCB polymer surface showing the effect of CMP with ILD1300 slurry and recipe I: (a) cured at 255 °C; (b) cured at 188 °C; (c) uncured. Quantitative data are shown in Table 6.

4. EBiS fabrication process

The EBiS process uses standard microfabrication tools and techniques including photolithography, reactive ion etching (RIE) or deep reactive ion etching (DRIE), and CMP. The process includes consecutive BCB deposition and planarization steps until the desired step height reduction (SHR) is achieved on the wafer. Obviously, the number of deposition and planarization steps depends on the desired size of the BCB islands, the desired thickness of the BCB polymer film, and the line of Cyclotene used. For instance, in case of the electrostatic micromotor, large island areas (e.g., 5 mm × 10 mm and larger), and a 25-μm thick BCB polymer film were required to achieve good electrical isolation [17]. In this case, two to three layers of Cyclotene 4026-46 were needed to completely fill the islands.

Fig. 4 shows the main steps in EBiS process. Starting from a silicon wafer, the island areas are patterned in photoresist and etched in silicon using conventional photolithography and RIE or DRIE as seen in Fig. 4(a). Silicon is etched as deep as required for the desired isolation (we have used RIE to etch 12-μm deep trenches and DRIE to etch 25-μm trenches on different test samples). The photoresist etch mask is kept until after deposition of the first BCB layer for lift-off of BCB ridges. Next, an adhesion promoter for BCB polymers, AP3000 is dispensed and spun onto the wafer. Photosensitive BCB is then dispensed, spun on and patterned over the etched islands as seen in Fig. 4(b). The BCB pattern area is chosen to be 100 μm larger on each side than the island area. This ensures that no void is developed inside the BCB islands. However, a BCB ridge forms around each island and needs to be removed. Before the planarization step, the photoresist is stripped in acetone inside an ultrasonic bath to facilitate lift-off of the BCB ridges around the islands and reduce the height of the ridges as shown in Fig. 4(c). This greatly increases the planarity of the wafer and helps with the planarization step. A short descumming in O_2/CF_4 plasma is also performed to remove any remaining BCB residue after development.

Planarization is the most important step in EBiS process. A short CMP is performed to remove the BCB ridges around the islands as shown in Fig. 4(d) and leaves a depression over the island area. Figs. 5 and 6 illustrate the removal of the 100-μm wide BCB ridges with optical micrographs and optical profilometry graphs of BCB islands before and after CMP. The uncured BCB ridges, as shown in Figs. 5 and 6(a), were completely removed after 5 min of CMP (recipe I with ILD1300 slurry). The average removal rate of the uncured BCB ridges was therefore higher than 1.6 μm/min. The exact removal rate could not be determined because the ridges might have been completely removed within a shorter polishing time. Considering the removal rate of the uncured

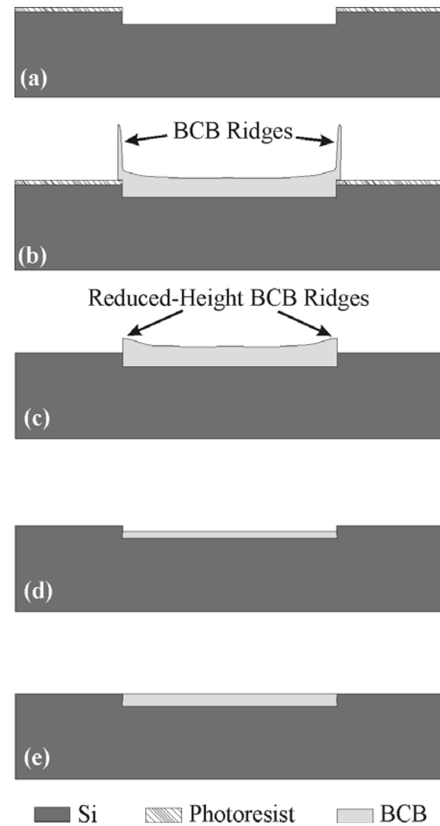

Fig. 4. Major fabrication steps of EBiS process: (a) DRIE of silicon to form islands; (b) spin-casting and patterning the first layer of photosensitive BCB polymer; (c) stripping photoresist, lifting off BCB ridges; (d) planarizing the BCB islands with CMP, and (e) repeat steps (b–d) for the second layer of photosensitive BCB polymer with partial-curing to fill and planarize the EBiS island.

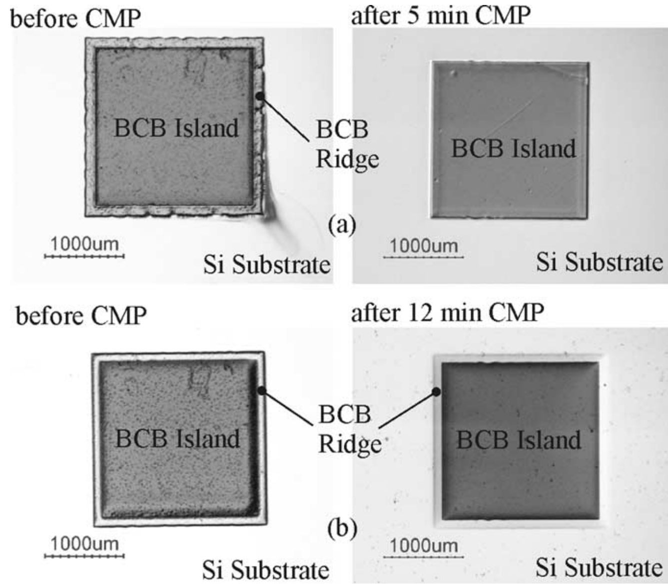

Fig. 5. Optical micrographs of two identical 2 mm × 2 mm EBiS islands on two samples before and after CMP with ILD1300 slurry and recipe I: (a) uncured, and (b) cured at 210 °C (standard soft cure).

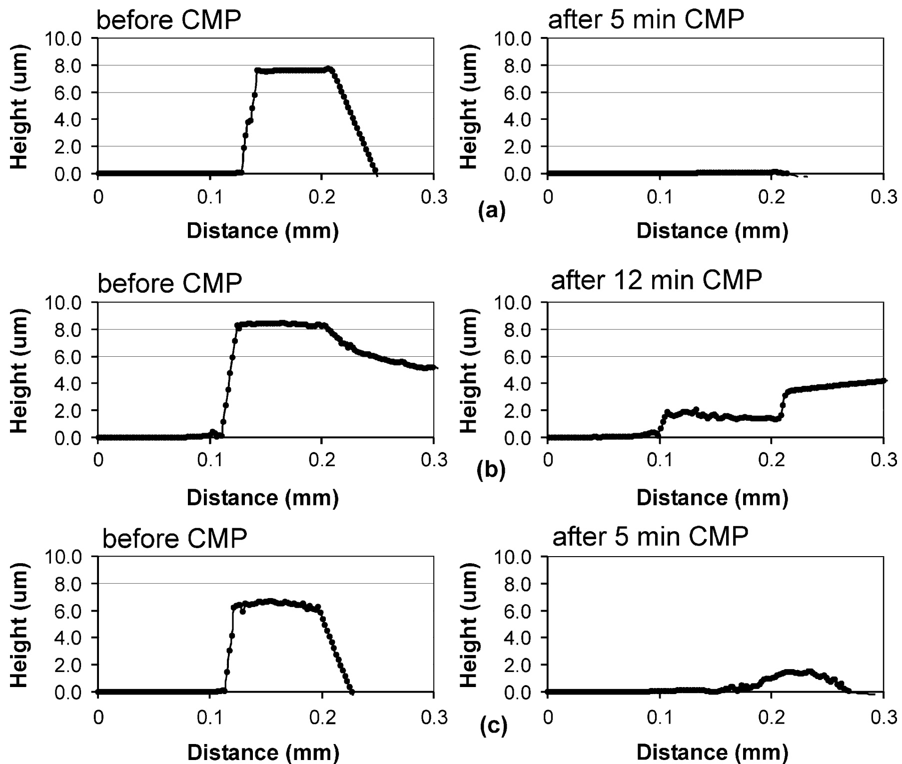

Fig. 6. Optical profiles of BCB ridges around three identical EBiS islands on three samples before and after CMP with ILD1300 slurry and recipe I: (a) uncured; (b) cured at 200 °C; (c) cured at 210 °C (standard soft cure).

blanket BCB film, as discussed in Section 3, about 2–3 min of polishing time should have been enough to remove the ridges.

In order to fill the depression, the second BCB layer is spun on and patterned. At this point, the films should be partially cured at a temperature close to the activation temperature of BCB polymerization. The curing helps with cross-linking of the BCB layers. If the cure temperature is too low, the top BCB layer is peeled off during the CMP. On the other hand, if the cure temperature is too high, the CMP removal rate of the BCB ridges is too low. However, since a ridge is mechanically weaker than a blanket film, the removal rate of cured BCB ridges is much higher than the removal rate of blanket films. As Figs. 5 and 6(b) show the soft-cured BCB ridges were not completely removed after 12 min of CMP (recipe I with ILD1300 slurry). The average removal rate was measured to be 0.3 μm/min. To further increase the removal rate of the ridges, the BCB film was cured at temperatures lower than the standard soft cure (210 °C). The removal of the 200 °C-cured BCB ridges, as shown in Fig. 6(c), was much faster, with an average removal rate of 0.9 μm/min. We were able to increase the removal rate of the cured BCB ridges up to 2.4 μm/min with no peel-off by lowering the cure temperature to 184 °C.

Finally, as shown in Fig. 4(e), the BCB islands are planarized using CMP, providing a planar surface for the subsequent process steps. Depending on the subsequent processes, a soft cure (at 210 °C for 40 min) or a hard cure (at 250 °C for 60 min) of BCB polymer is performed at the end of the process. Fig. 7 shows scanning electron micrographs (SEMs) of the cross-section of a completed EbiS island. The island is 12 μm deep with an area of 5 mm × 10 mm.

In order to study how the planarity of the EBiS islands evolves during the fabrication, we measured the island depth and the BCB ridge height before and after each BCB film deposition and before and after each CMP run. The measurement was performed on four wafers (A, B, C, and D) with islands of two different sizes, 5 mm × 14 mm and 5 mm × 20 mm. The islands were etched using DRIE to an average depth of 26.8 μm. Fig. 8 shows how the average island depression depth in each wafer changes after each step. Two layers of BCB polymer were deposited and three CMP runs were performed. The average island depression depth was reduced to below 2 μm. It is clear from the trend of reduction in the depression depth that with another BCB layer deposition and CMP run, the average island depression can be reduced to close to zero. Although the mechanical abrasion is negligible in a depression, an increase in the depression depth is observed after each CMP step. This shows that ILD1300 slurry can chemically remove BCB polymer from the island area. Fig. 9 shows the changes of the average BCB ridge height in each wafer after each step.

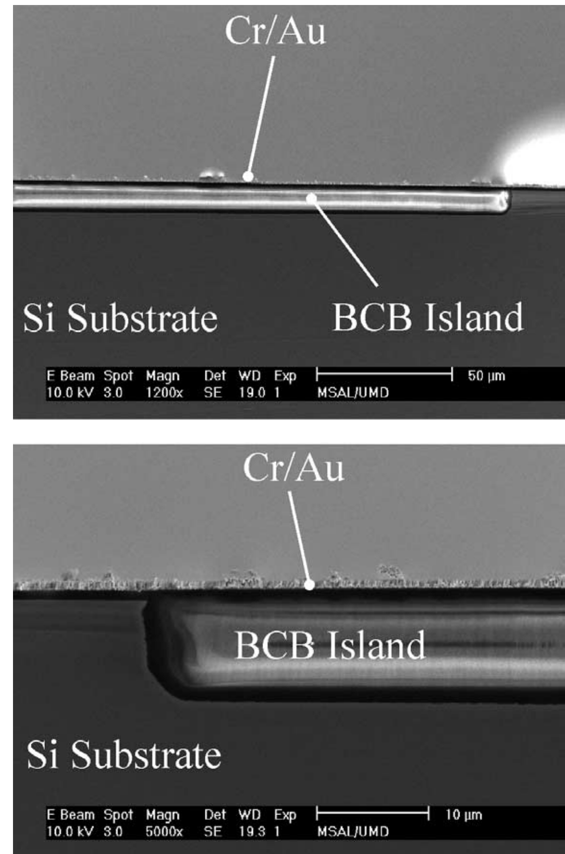

Fig. 7. Scanning electron micrographs (SEMs) showing the cross section of a 5 mm × 10 mm, 12-μm deep EBiS island after deposition of two BCB layers and planarization. Thin layers of chromium (Cr) and gold (Au) were sputtered on the wafer to help with taking the SEM and to test the adhesion of metal layers.

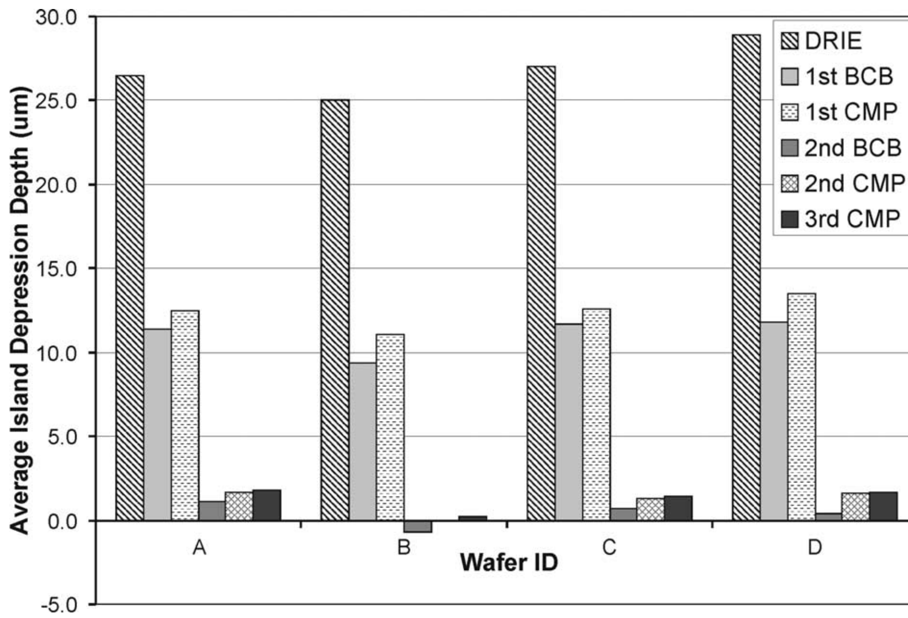

Fig. 8. Average island depression in different steps of EBiS process for four test wafers.

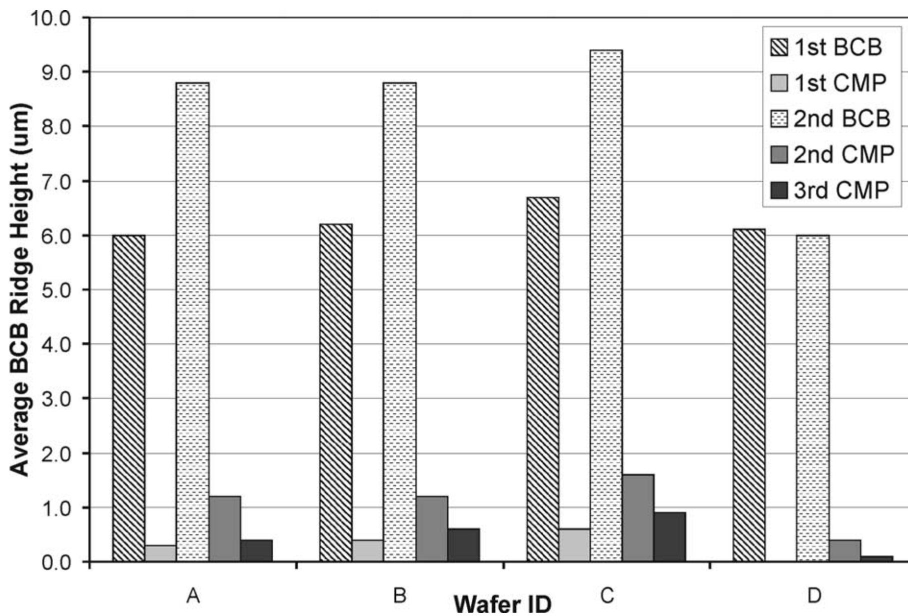

Fig. 9. Average BCB ridge heights in different steps of EBiS process for four test wafers.

The average height was reduced to less than 1 μm and could be reduced even more with a longer CMP at the end. In order to quantify the planarization of the EBiS process, we calculated the total step height reduction (T-SHR) in each step for each wafer. T-SHR is given by

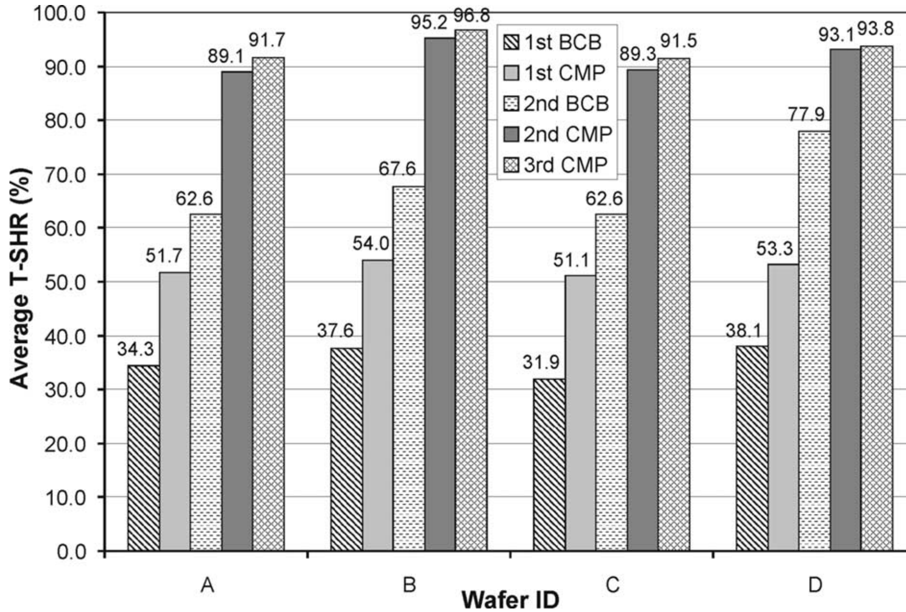

Fig. 10. Average total step height reduction (SHR) in different steps of EBiS process for four test wafers.

$$\text{T-SHR} = \left(1 - \frac{h_{\text{Ridge}} + d_{\text{Dep}}}{d_{\text{island}}}\right) \times 100, \quad (3)$$

where h_{Ridge} is the average BCB ridge height, d_{dep} is the average island depression depth, and d_{island} is the average initial island depth. The ideal T-SHR is 100%, which represents perfectly planarized EBiS islands. As shown in Fig. 10, a T-SHR of above 90% was achieved for all wafers. The T-SHR of wafer B is even above 95%. Considering the increase in T-SHR from second to third CMP, a T-SHR of close to 100% could be accomplished with longer CMP at the end.

5. Conclusion

In this paper, we presented the EBiS process, a fabrication method to develop planarized isolated islands of thick BCB polymer embedded in a silicon substrate. These islands can provide electrical isolation integrated with silicon MEMS, such as electrostatic micromotors and microgenerators. CMP of BCB, a key step in EBiS process was characterized and the effect of cure temperature on CMP removal rate, non-uniformity, and surface roughness of blanket BCB films was investigated. It was found that the removal rate increases when cured at lower temperatures. However, this is gained at the expense of an increase in non-uniformity, surface roughness, scratch density, and embedded particles. It was observed that the removal rate of the BCB ridges was much higher than the removal rate of the blanket film. A combination of uncured and partially cured BCB was used to increase the removal rate of the BCB ridges in the EBiS process and a planarization of more than 95% was achieved. The EBiS process can be used in many different MEMS and microsystem applications to provide electrical and thermal isolation.

Acknowledgments

This work is supported by the National Science Foundation (NSF) under Grant No. ECS-0224361. This work is also supported by the Army Research Office (ARO) through MAV MURI Program (Grant No. ARMY-W911NF0410176) with Technical Monitor as Dr. Gary Anderson. The authors would like to thank Nitta Haas Incorpo-

rated for supplying the ILD1300 slurry and polishing pads. We would also like to thank Mr. Thomas C. Loughran and Mr. Nolan A. Ballew for help with fabrication, Mr. Wen-Hsien Chuang for help with the SEM pictures, and Dr. Madhumita Datta for help with the AFM measurements, all from University of Maryland.

References

[1] A.H. Epstein, et al., in: Digest Tech. Papers 9th International Conference Solid-State Sensors and Actuators (Transducers'97), 1997, pp. 753–756.
[2] A.H. Epstein, et al., in: Proceedings of the Eighth International Symposium on Transport Phenomena and Dynamics of Rotating Machinery (ISROMAC'8), 2000.
[3] R. Ghodssi, et al., in: Digest Tech. Papers 10th International Conference on Solid-State Sensors and Actuators (Tansducers'99), 1999, pp. 1456–1459.
[4] X. Zhang, et al., in: Solid-State Sensor and Actuator Workshop, 2000, pp. 316–319.
[5] K.-S. Chen et al., J. Micromech. Microeng. 12 (2002) 714–722.
[6] M. Raieszadeh, et al., in: Proceedings of the 18th International Conference on Micro Electro Mechanical Systems (MEMS'05), 2005, pp. 199–202.
[7] G. Barillaro et al., Sens. Actuat. A 107 (2003) 279–284.
[8] C. Zhang, K. Najafi, J. Micromech. Microeng. 14 (2004) 769–774.
[9] A. Modafe et al., IEEE Trans. Dev. Mater. Reliab. 4 (2004) 495–508.
[10] R.A. Kirchhoff, K.J. Bruza, Prog. Polym. Sci. 18 (1993) 85–185.
[11] M.F. Farona, Prog. Polym. Sci. 21 (1996) 505–555.
[12] M.E. Mills et al., Microelectron. Eng. 33 (1997) 327–334.
[13] T.-K.A. Chou, K. Najafi, in: Digest Tech. Papers 11th International Conference on Solid-State Sensors and Actuators (Tansducers'01), 2001, pp. 1570–1773.
[14] S. Guo, Proc. SPIE VII (2003) 422–429.
[15] N. Ghalichechian et al., J. Vac. Sci. Technol. B 22 (2004) 2439–2447.
[16] A. Modafe, et al., in: MRS Spring Meeting: Chemical–Mechanical Planarization – Integration, Technology, and Reliability Symposium, 2005.
[17] A. Modafe, et al., in: AVS 51st International Symposium, 2004.
[18] J.M. Steigerwald et al., Chemical Mechanical Planarization of Microelectronic Materials, Wiley, New York, 1997.
[19] C.L. Borst et al., Chemical–Mechanical Polishing of Low Dielectric Constant Polymers and Organosilicate Glasses, Kluwer Academic Publishers, Dordrecht, 2002, p. 48.
[20] J.M. Steigerwald et al., Chemical–Mechanical Planarization of Microelectronic Materials, Wiley, New York, 1997, p. 49.
[21] N.J. Brown et al., Proc. SPIE (1981) 42–57.
[22] F.G. Shi, B. Zhao, Appl. Phys. A 67 (1998) 249–252.
[23] T.K. Doy et al., J. Electrochem. Soc. 151 (2004) G196–G199.
[24] Y.-R. Jeng, P.-Y. Huang, Electrochem. Solid-State Lett. 7 (2004) G40–G43.
[25] Q. Luo et al., Thin Solid Films 335 (1998) 160–167.
[26] E. Paul, J. Electrochem. Soc. 148 (2001) G355–G358.
[27] E. Paul, J. Electrochem. Soc. 149 (2002) G305–G308.
[28] E. Paul, R. Vacassy, J. Electrochem. Soc. 150 (2003) G739–G743.
[29] S. Thagella et al., J. Electrochem. Soc. 151 (2004) G205–G215.
[30] J.M. Neirynck, in: Proceedings of the 23rd International Conference on Metallurgical Coatings and Thin Films: Thin Solid Films, 1996, pp. 447–452.
[31] R.W. Johnson et al., IEEE Trans. Compon. Hybrid Manufact. Technol. 13 (1990) 347–352.
[32] D.C. Burdeaux et al., J. Electron. Mater. 19 (1990) 1357–1366.